

# Motion pattern-based image features for glaucoma detection from retinal images

K Sai Deepak\*  
CVIT, IIIT Hyderabad  
Hyderabad, India  
sai.deepak@research.iiit.ac.in

Madhulika Jain  
CVIT, IIIT Hyderabad  
Hyderabad, India  
madhulika.jain@students.iiit.ac.in

Gopal Datt Joshi  
CVIT, IIIT Hyderabad  
Hyderabad, India  
gopal@research.iiit.ac.in

Jayanthi Sivaswamy  
CVIT, IIIT Hyderabad  
Hyderabad, India  
jsivaswamy@iiit.ac.in

## ABSTRACT

Glaucoma is an eye disorder that causes irreversible loss of vision and is prevalent in the aging population. Glaucoma is indicated both by structural changes and presence of atrophy in retina. In retinal images, these appear in the form of subtle variation of local intensities. These variations are typically described using local shape based statistics which are prone to error. We propose an automated, global feature based approach to detect glaucoma from images. An image representation is devised to accentuate subtle indicators of the disease such that global image features can discriminate between normal and glaucoma cases effectively.

The proposed method is demonstrated on a large image dataset annotated by 3 medical experts. The results show the method to be effective in detecting subtle glaucoma indicators. The classification performance on a dataset of 1186 color retinal images containing a mixture of normal, suspect and confirmed cases of glaucoma is 97 percent sensitivity at 87 percent specificity. This improves further when the suspect cases are removed from the abnormal cases. Thus, the proposed method offers a good solution for glaucoma screening from retinal images.

## Keywords

Color retinal image, Glaucoma, Global image features, Abnormality detection, GMP

## 1. INTRODUCTION

Glaucoma is among the most common causes for loss of vision due to eye related disorders. It occurs typically in the aging population of urban regions in the world and is estimated to affect nearly 79 million people by the year 2020

\*Corresponding author

Permission to make digital or hard copies of all or part of this work for personal or classroom use is granted without fee provided that copies are not made or distributed for profit or commercial advantage and that copies bear this notice and the full citation on the first page. To copy otherwise, to republish, to post on servers or to redistribute to lists, requires prior specific permission and/or a fee.

ICVGIP '12, December 16-19, 2012, Mumbai, India  
Copyright 2012 ACM 978-1-4503-1660-6/12/12 ...\$15.00.

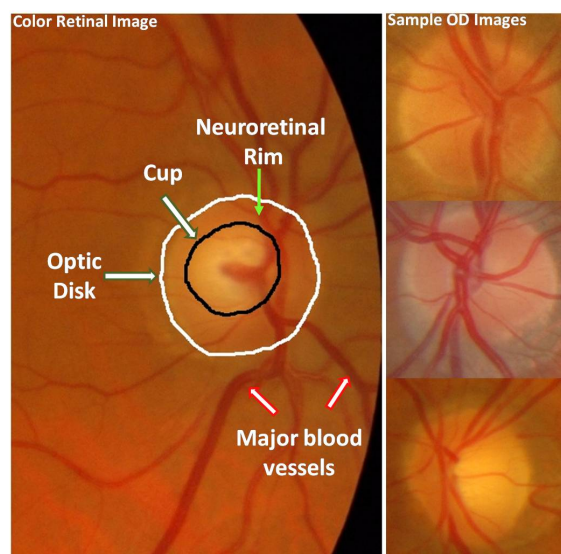
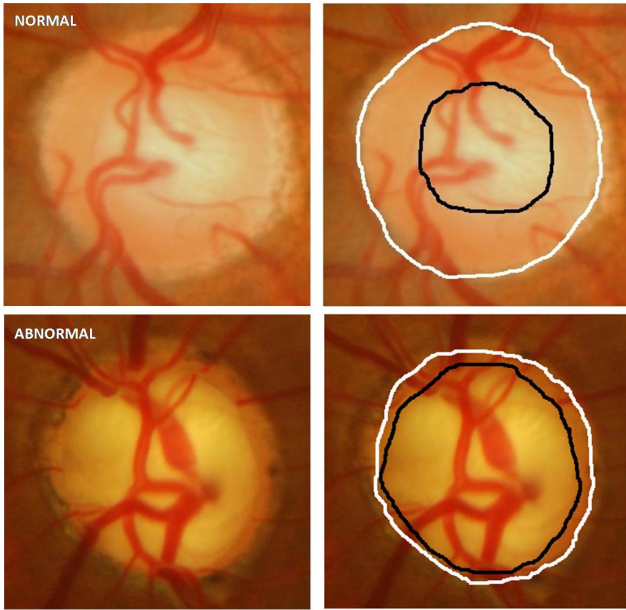


Figure 1: Sample color retinal image and optic disc regions. Left: a part of the retinal image containing structures of interest is shown with annotated optic disc and other retinal structures. Right: Variations in color, texture, disc boundary shape and surrounding deformations found typically in optic disc regions.

[2][8]. Untreated glaucoma leads to irreparable damage to retina while detecting it in the early phases helps in curbing its development through proper medication. Color retinal imaging has become the *de facto* standard for screening the presence of different types of retinopathy due to its low cost and ease of use [11]. Therefore, screening for the presence of glaucoma by classifying retinal images as normal and glaucomatous is a problem of clinical significance in population screening.

The problem of automatic glaucoma detection from retinal images has been an active area of research for a decade now [1][4][8][10][3]. Color retinal images provide 2-D projection of retina yielding structural information of optic disc (OD) along with other retinal structures (shown in figure



**Figure 2: Sample normal and Glaucomatous OD depicting the effect of rim thinning due to the disease (left to right). Expert marking in black is used for depicting cup and white for disc boundary.**

1). Of these, OD and the region in its vicinity are of interest for glaucoma. An OD region consists of two structures: the *disc* identified by the outer boundary of OD (marked in white) and the *cup* which is within the inner boundary of OD, along the bend in blood vessels (marked in white).

Glaucoma leads to structural changes in the OD resulting in deformation of normal cup and disc morphology. A common deformation is the enlargement of cup with respect to the disc and is referred to as cupping. Such morphological changes during disease progression is quantified using shape metrics like cup-to-disc ratio (area, diameter) [9] [8]. Therefore, detecting cup and disc boundary automatically is a necessary task for automatic glaucoma detection.

A significant body of work in retinal image analysis focus on detection and segmentation of optic disc and cup [1][4]. Figure 2 shows normal and glaucomatous OD regions of the retinal image with their respective cup and disc boundaries. Segmentation and identifying these ill-defined boundaries is a difficult task as just local intensity based statistics are insufficient to discriminate between OD, cup and neighboring deformations [9]. In the clinical setting, 3D nature of the cup is used by experts to gauge the cup boundary. Since quantification of glaucoma depends heavily on the accuracy of segmentation, this approach to automatically detect glaucoma is extremely challenging.

In contrast to segmentation-based approach, another approach to glaucoma detection has been to use *global* image features around OD for normal and disease classification [10][2][3]. This approach assumes that the morphological changes in OD caused by the disease, can be encoded using global image features, thereby removing the need to identify cup and disc boundaries accurately. Consequently, limitations of segmentation based techniques of glaucoma detection are eliminated. Given a region of interest around OD

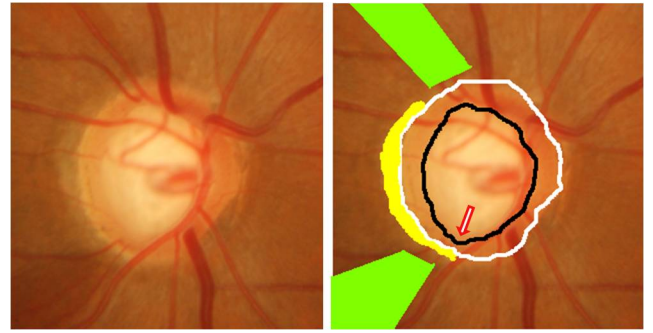


**Figure 3: Glaucomatous case depicting local rim thinning (with red arrow), PPA (marked in yellow) and RNFL defect (marked in green).**

in the retinal image, a vessel-free image is first generated by roughly segmenting and inpainting the blood vessels [2] [3] to suppress deviations in global feature characteristics due to structural variations within normal images. Various statistics based on color, intensity and texture are computed to encode features for each image. Supervised classification is performed to separate normal from disease cases.

Global features are usually implemented to describe easily identifiable global characteristics in medical images [12]. Therefore there are certain pitfalls in using global image features for describing certain pathology in medical images.

1. Global image features are insufficient for encoding subtle local deformations in anatomical shape or highly localized change in intensity distribution due to pathology. Such localized change mandate the use of local image features to identify presence or absence of abnormality at image level [12].
2. It may be possible to encode certain localized pathology using global image features by first applying local filters that enhance intensities in the affected pixels. Such methods also run the risk of encoding intra-class variations in intensity, tissue pigmentation and normal anatomical shape, which is significant in retinal images [6].
3. There is always a risk of adapting image features for a particular image dataset through transformations like Principal Component Analysis. The resultant features may identify global parameters discriminating between the normal and abnormal classes, while failing to encode subtle disease indicators. Suspect glaucoma cases in general are quite close to normals, only exhibiting subtle variations, and hence will be classified as normal.

Bock et al. [10] presented a pre-processing solution to remove disease independent variations that occur in retinal images. A polynomial surface fitting operation is performed to normalize large intensity variations in retina followed by vessel suppression. On a test set of 100 images, such pre-processing (before feature extraction) was shown to improve detection of normal cases. However, only a slight improvement in detection of disease cases was observed.

In this paper, we present a new approach based on global image features for classifying glaucoma in color retinal images. The proposed method is robust to the presence of

local and global intensity variations across images and is also sensitive to subtle disease indicators, in suspect cases. The underlying strategy first spatially extends the relevant local deformations within the image by applying appropriate transformations [5]. This gives rise to a new image representation which provides significant differentiation between the normal and glaucomatous image classes. The obtained representation aids in encoding global and local image variations in a unified way and therefore gives high detection sensitivity even for subtle disc deformations. In addition, we model the feature sub-space for normal cases by utilizing the similarity shared by normal retinal images. In such a feature space, intra-class distance between normal cases should be low as compared to the inter-class distance between normal and abnormal cases. In short, we extend the scope of the transformation proposed in [5] to the problem of detecting abnormalities caused by subtle morphological changes. The rest of the paper is organized as follows. Section 2 describes the proposed method in detail. This is followed by the a description of the experimental setup used and obtained results in section 3. The paper is concluded in section 4 with a detailed discussion.

## 2. PROPOSED METHOD

Glaucoma affects the optic nerve head and surrounding regions in retina which can be observed in color retinal images. Therefore given a retinal image, a region of interest (ROI),  $I$  is first extracted around the OD automatically. We try to derive a representation of the retinal image such that the resulting image features are more meaningful for classification. In order to implement this approach, we extend a recently proposed image representation, namely the Generalized Moment Pattern (GMP) [5]. By transforming the given ROI to a GMP ( $I_{GMP}$ ), we ensure that the spatial extent of intensities corresponding to the signal of interest (abnormalities) within an image is accentuated, whereas other background intensities remain unchanged or are attenuated. Next, suitable global image features are extracted on  $I_{GMP}$  for classification. A one-class classifier is used to learn the feature sub-space corresponding to normal images and classify new images as normal and glaucoma cases respectively.

Next, we list visual indicators of glaucoma in detail and identify necessary image representation for enabling extraction of global image features from ROIs.

### 2.1 Deriving Image Representation

A normal optic disc in a color retinal image is characterized by two low contrast, concentric, roughly- circular structures, the disc and cup (see figure 2). The region between boundaries of these two structures is known as the neuroretinal rim. As glaucoma starts affecting retina, morphological changes occur within these two structures. Additional indicators of glaucoma also arise around the OD region in the form of subtle variations in intensity and texture. We use these observations to derive relevant features for describing both normal and abnormal (glaucoma) cases.

#### 2.1.1 Glaucoma Indicators in Retinal Images

**Neuroretinal Rim Thinning** in a retinal image is a definite indicator of glaucoma. The rim begins to thin with the onset of disease as the cup boundary starts approaching the disc. As a result the cup-to-disc ratio increases. Thinning can be a global or local phenomenon around the cup bound-

ary. Figure 2 shows an example of global rim thinning in the second row. It can be noted that nearly the entire boundary along the cup is extended to the disc in this case resulting in the diagnosis of *confirmed glaucoma*. Figure 3 shows an example where only a small local region in the rim has undergone thinning. Here, thinning is a subtle variation in the ill-defined cup boundary. While easily visible to a trained human eye, encoding such minor variations across retinal images, already inflicted with other non-disease variations is a significant challenge.

**Peripapillary Atrophy (PPA)** is another indicator for glaucoma (see figure 3). While the cup boundary is not affected due to this, a change in intensity can be observed clearly adjoining the disc boundary. PPA occurs due to atrophy of retinal cells around optic disc. Some atrophy appears in both normal and glaucomatous eyes but it is more commonly observed closer in glaucomatous cases. We can observe that an increase in brightness outside the disc boundary appears in the PPA affected pixels in comparison to normal retina. Similar to rim thinning, PPA appears as a subtle variation in the disc boundary and it is even difficult for a human observer to differentiate affected regions from normal tissues.

**Retinal Nerve Fibre Layer (RNFL) defect** is the most subtle visual indicator of glaucoma in retinal images and occurs due to the loss of the respective layer in retina. It appears roughly as a wedge-shaped region characterized by a loss in brightness in the peri-papillary regions in retinal images (see figure 3). Visual examination is performed by doctors for typically identifying striations, sudden reduction in brightness and increased clarity of blood vessels.

We primarily focus on the first two indicators for deriving the required image representation while validation is performed for images also containing RNFL defect.

#### 2.1.2 GMP for Detecting Bright Lesions

GMP has been proposed and utilized to detect abnormalities, specifically hard exudates which appear as localized bright lesions in retinal images [5]. The underlying assumption with GMP is that a lesion appears as a contrasting disturbance in local intensities against the normal background within the retinal image. Motion is induced in an image to observe the blurring effect of a moving object within a scene. This effect serves spatially spread and thus accentuate intensities corresponding to high contrast lesions over normal background.

Motion is simulated in a static image by applying a rigid transformation in steps, with center of the image as origin. The transformation results in generation of several samples at each 2-D location. The sample values (Intensities) at each location are coalesced to generate the desired GMP (see figure 4).

Given a region of interest  $I(\bar{p})$ , a GMP  $I_{GMP}$  is generated as follows:

$$I_{GMP} = f(R(I(\bar{p}))) \quad (1)$$

$\bar{p}$  denotes a location in the 2-D ROI and  $R$  is a rigid transformation applied to generate a sequence of transformed images and  $f$  is the coalescing function. Further details on GMP generation can be found in [5].

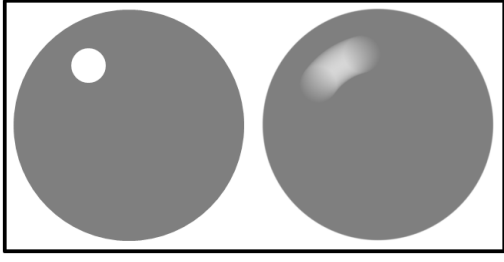


**Figure 4: Image with simulated bright lesion (left) and corresponding GMP image (right) obtained by inducing rotation to the original image.**

### 2.1.3 Image Representation for Glaucoma Detection

We propose to extend the use of GMP to our problem of differentiating between normal and glaucomatous retinal images. Normal ROI (the OD region) generally has a uniform structural behavior with the presence of cup and disc boundaries. In the absence of 3-D information, experts use vessel bends in the OD region of a retinal image to identify the cup boundary point and extrapolate it along with other cues such subtle change in color. The glaucoma affected ROI is devoid of the subtle cup boundary due to thinning of the neuroretinal rim. The loss of OD boundary definition is also seen in the presence of PPA. Thus, unlike the bright lesion detection problem in [5], using GMP for glaucoma detection has various challenges:

1. Glaucoma appears as a subtle change in the structure of cup and disc boundary. Consequently, the strategy proposed in [5] namely, using a normal background as a reference and smearing the intensities corresponding to the abnormality to generate a GMP is inadequate. Such a strategy will instead serve to suppress subtle glaucoma indicators like localized rim thinning.
2. Detection of hard exudates through GMP relies on the rotational (about the center of the image) symmetry in normal images which is lost when a lesion is introduced. Rotational symmetry is nearly intact for both the normal and abnormal OD in the case of glaucoma.
3. It can be observed from figure 2 that the relative contrast of cup and disc is not consistent along the cup boundary for both the normal and abnormal cases. Therefore selection of GMP parameters need to be consistent with the best indicator of abnormality along the nearly circular cup boundary to detect local thinning.

Choice of motion parameters used to generate GMP should reflect the features of interest in the ROI. The following parameters are identified for generating required moment pattern.

**Coalescing function:** Local contrast between various structures, cup, disc, PPA and RNFL defect is observed to be a consistent feature in abnormal retinal ROIs. Since these variations are subtle in most boundary pixels, the coalescing function of maximum ( $I_{GMP} = \max(R(I(\vec{p})))$ ) is used in order to achieve the best separation between various abnormal structures. Using an averaging operation will lead to loss of any perceivable differences between the structures.

**Motion Parameters:** Since the neuroretinal rim is roughly annular in shape, it is convenient to apply rotational motion.

We propose to choose the pivot of rotation in such a manner as to accentuate the subtle structural variation in glaucoma. Shifting the pivot from the center of ROI to its outer edge will accentuate any asymmetry in the cup-disc morphology. This is shown with synthetic models of the ROI for different cases in figure 5. Here, the first row shows the normal, suspect and confirmed cases of glaucomatous OD. The suspect and confirmed cases of glaucoma have increasing cup size with respect to the normal OD. This ROI is rotated about the pivot shown as a red dot and the resulting samples are coalesced with a maximum function. The generated GMPs are shown in the second row of figure 5. It is clear that any change in the neuroretinal rim morphology is reflected in the GMPs as a change in the relative distribution of bright and grey pixels. The rim appears to be spatially enhanced in the normal case as opposed to suspect and abnormal cases. This accentuated effect of cup/rim region in the GMP of glaucoma cases can be used by the image descriptors for classification. The interesting thing to note is that even a local rim thinning (last column) is captured by the GMP and is distinguishable from the normal case. The above motion pattern will also be able to accentuate the changes that occur due to the presence of PPA, as a distinctive smear pattern on the periphery of optic disc.

**Pivot of Motion:** In theory, the pivot of rotation can be placed anywhere on the boundary of OD. We have observed that Ophthalmologists prefer to measure the vertical cup-to-disc diameter ratio for assessment of glaucoma. Hence, it is preferable to choose the pivot on the left or right end of the OD boundary, if thinning in vertical direction is more likely. In our work, the pivot of rotation was located on the left side of the ROI similar to the synthetic example in Figure 5.

The proposed GMP-based representation for glaucoma detection is as follows:

$$I_{GMP}(\vec{p}) = \max_{n=[0 \dots (N-1)]} R_{\theta_n}(I(\vec{p} - \vec{c})) \quad (2)$$

where  $R_{\theta}$  is a rotation matrix and  $\vec{c}$  is the pivot location. The rotation is applied in steps to generate a set of  $n = 0, \dots, N - 1$  frames.  $\theta_n = n\theta_0$  denotes the extent of rotation in the  $n^{th}$  frame.  $\theta_0$  is the rotation step.  $\theta_0 = 40^\circ$  and  $N = \frac{360^\circ}{\theta_0}$  have been used for figure 5. The rotation step was identified experimentally.

Locating the pivot on the periphery for a roughly circular ROI will result in a GMP which is larger than the ROI. For an ROI  $I$  of size  $m \times m$ , the resultant transformed image  $I_{\theta_n}$  will be double the original size:

$$I^{m \times m} \xrightarrow{R_{\theta_n}} I_{\theta_n}^{2m \times 2m}$$

Missing values in the transformed ROI  $I_{\theta_n}^{2m \times 2m}$  are zero padded. As shown in equation 2, the transformed images are coalesced using a maximum operation to generate the GMP response. This maximum operation will reject zero values in the presence of samples from ROI. Next, we describe in detail the feature extraction from the GMP and the classification steps used.

## 2.2 Feature Extraction and Classification

GMP representation of a normal case results in accentuation of intensities corresponding to the larger neuroretinal

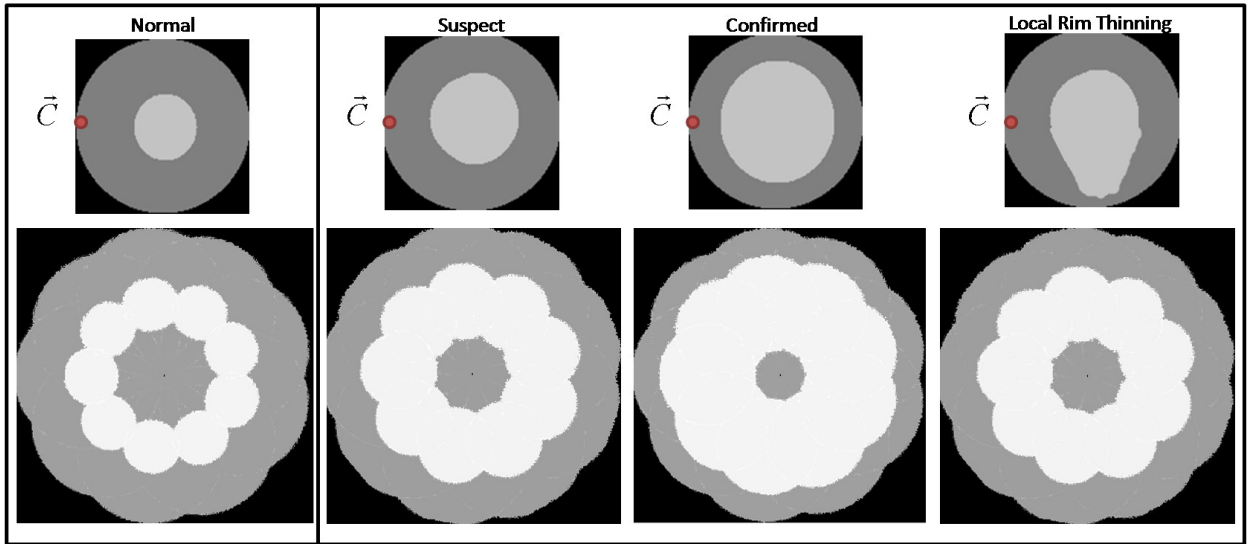


Figure 5: (first row) Synthetic ROIs simulating normal and glaucomatous OD region. (second row) rotational GMPs. The pivot for rotation is indicated by a red marker.

rim. This behavior is consistent in normal OD across retinal images. Therefore features derived on the normal images should result in a compact sub-space due to the uniformity of GMP among normal cases. We derive two image descriptors for describing the GMP responses. The first descriptor is based on Radon transform as proposed in [5]. A second image descriptor considered is based on histogram of pixel intensities where the intensities are binned for generating feature vector with fewer dimensions.

**Radon Transform based Descriptor (RTD):** Given an image, its Radon transform is the projection of intensities along a line oriented at direction  $\alpha$ .  $\alpha$  is the angle between the lines of projection and the  $x$  axis. We obtain a feature vector for the image  $I_{GMP}$  by concatenating the projections for different values of angle  $\alpha$ . The feature vector is normalized to address variation in the sizes of OD that occur across patients.

Accentuated spatial extent of neuroretinal rim in  $I_{GMP}$  of normal cases is reflected in the projection based feature vector. A large neuroretinal rim for normal OD will exhibit a shorter width of the intensity hill in 1-D projection in comparison to glaucomatous OD.

**Histogram of Intensity Clusters (HIC):** GMP response of all retinal ROIs are generated and normalized to have values between [0-1]. An intensity based clustering is performed for all GMP responses using k-means algorithm. Based on the contrast of various structures, intensities corresponding to cup, disk and PPA are expected to fall in different clusters. A histogram of intensities for each ROI corresponding to these clusters is used as the feature vector.  $k$  denotes the length of feature vector and it is identified empirically.

Further, the derived feature vectors are used for learning normal cases for the task of one-class classification. Since some homogeneity exists among the features for normal cases, a linear sub-space is sufficient for describing the normal sub-space. A new image is considered as normal if it lies close to this sub-space otherwise it is classified as abnormal. Principal Component Analysis Data Description (PCA-DD), is

used for the one-class classification of retinal images [5]. An empirically determined threshold is used to identify the closeness of a new image to the normal sub-space. Next, we discuss the results of applying the proposed image representation and feature descriptors on publicly available benchmarked datasets.

### 3. EXPERIMENTS AND RESULTS

The experiments for assessing the proposed method is performed on a dataset of color fundus images. The desired ROI is extracted and preprocessed as explained below. The optimal rotation step for generating GMP representation is identified as the one that provides maximum separation between normal and abnormal cases. Next, motion (with the optimal parameters) is induced to the ROIs to generate GMPs. A PCA-DD classifier is trained on a set of *normal* training images using the feature extracted from the GMPs. Two global image descriptors, RTD and HIC are considered for the feature. The classification performance is evaluated on a set of test images (normal and abnormal).

#### 3.1 Dataset

An annotated dataset of color retinal images was collected from 596 patients (1192 eyes/images). The size of each image is 1494x1996 pixels. Ground truth for the dataset was collected from 3 experts with image level annotation as normal, suspect and confirm case of glaucoma. A gold standard for the expert annotation was found using a majority voting on the decision by experts. Cases where no consensus could be found were removed from experiments. The resultant dataset consists of 624 image for normals, 234 corresponding to suspect cases and 328 as confirmed cases of glaucoma. For our experiments on classification of glaucoma cases against normals, we divided the gold standard data into two sets: *Set1* consisting 624 images in the normal class and 562 (234 suspect + 328 confirmed glaucoma) images in the abnormal class. *Set2* consisting 624 images in the normal class as before and only 328 images (only confirmed cases) in the

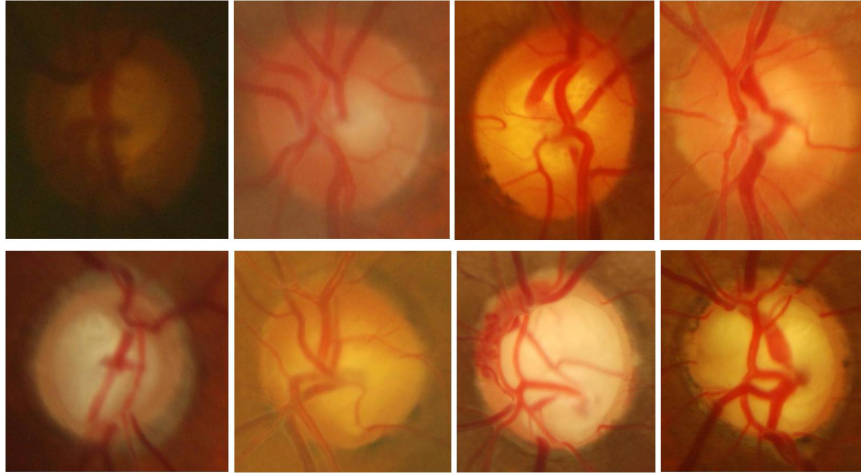


Figure 6: Sample normal and glaucomatous ROI images. First row: normal cases. Second row, left to right: 2 suspect and 2 confirmed glaucoma cases.

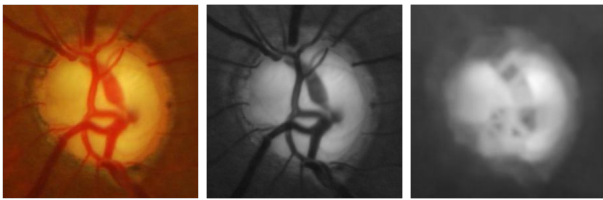


Figure 7: Effect of vessel suppression on the original ROI (left), its green channel (middle) and vessel suppression result (right).

abnormal class.

Some sample images of normal, suspect and confirmed cases from the dataset are shown in figure 6 to show the level of difficulty in differentiating between the normal and abnormal cases through visual inspection.

### 3.2 Region of Interest Extraction

A rectangular ROI around OD is extracted using the method in [6] for further processing. The green channel of the image is used as it provides good contrast among various retinal structures [13]. The center of the OD and its radius ( $r$ ) is then identified using the method proposed in [6]. Some of the background region in the retinal image is also retained along with OD, in the rectangular ROI so that the abnormalities in the background region (PPA, RNFL) can also be accounted for in the GMP. We extract an ROI with  $r + 45$  pixels in this work.

The ROI is pre-processed before generating GMP representation. Blood vessels in the region are detected using the method in [7]. Once all the vessels are identified, they are suppressed through inpainting. Result of automatic vessel detection and suppression can be seen in figure 7.

### 3.3 Image Representation & Descriptor

GMP representation for the extracted ROIs are generated using  $\theta_n = 360^\circ$  and maximum as the coalescing function. First, we observe the effect of increasing rotation step  $\theta_o$  on the classification accuracy for normal and abnormal images.

Dataset *set2* is used for this experiment. 324 normal im-

Table 1: Classification performance with RTD feature for varying rotation steps. Rotation step of 40 degrees provides best classification between normal and glaucoma cases.

Rotation Step	Area Under Curve
$20^\circ$	0.45
$30^\circ$	0.56
$40^\circ$	0.98
$50^\circ$	0.69

Table 2: Classification performance of normal and abnormal (containing both suspect and confirmed glaucoma) retinal images.

Experiment	Sensitivity	Specificity	AUC
RTD	0.97	0.87	0.96
HIC	0.84	0.67	0.81

ages are used for training the classifier while the remaining images are used for testing. The RTD descriptor is used to derive feature vectors from the GMPs. The feature vector is derived with a  $30^\circ$  resolution containing 6 bins each, resulting in a  $(180^\circ/30 = 6) \times 6 = 36$ -long vector.

Classification is performed using the PCA-DD classifier. The derived feature vectors are projected onto 6 dimensions to compute the reconstruction error. Normalized threshold ranging from 0 to 1 was applied on the error to generate sensitivity and specificity of detecting the glaucoma cases against normal ROIs. Here, sensitivity indicates the successful detection of images with glaucoma while specificity corresponds to correctly identifying the normal images.

Classification performance with various values of  $\theta_o = 20^\circ, 30^\circ, 40^\circ$ , and  $50^\circ$  is shown in table 1. Sensitivity and specificity of the classification task is plotted as a Receiver Operating Characteristic (ROC) curve. The best parameter value is identified as the one resulting in the highest Area Under the ROC Curve (AUC). We can observe that the rotation step of  $\theta_o = 40^\circ$  yields the highest AUC. Hence, this is used for assessment of classification task in the rest of the

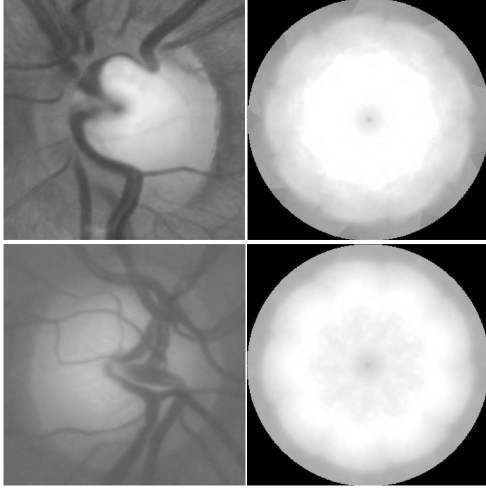


Figure 8: Sample ROIs (left column) and their GMP (right column). Normal case (first row) Glaucomatous case (second row).

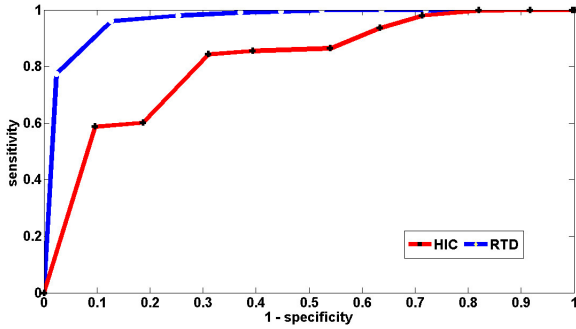


Figure 9: ROC curves for classification of normal against suspect + confirmed cases of glaucoma.

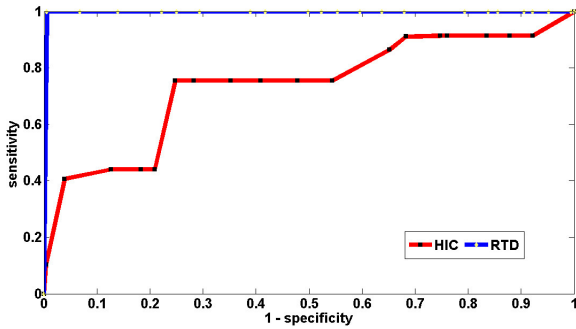


Figure 10: ROC curves for classification of normal against confirmed cases of glaucoma.

Table 3: Classification performance of normal and confirmed glaucoma retinal images.

Descriptor	Sensitivity	Specificity	AUC
RTD	1	0.98	0.98
HIC	0.75	0.78	0.7

Table 4: Comparison of the proposed method with methods in literature. Sens- Sensitivity, Spec- Specificity, Avg- Average.

Method	Images	Sens	Spec	Avg AUC
Proposed	952	1	0.99	0.99
Bock et al. [3]	575	0.73	0.85	0.88

experiments.

GMPs for a normal and an abnormal ROI with are shown in figure 8. We can observe a clear separation between the GMPs due to rim thinning. Next, we further analyze the classification results in detail for the two global image descriptors on datasets *set1* and *set2*.

### 3.4 Classification experiments

Two experiments are performed to evaluate the classification performance of the proposed method. They were to assess the ability to distinguish between i) normal and suspect+confirmed glaucoma cases (*set1*) and ii) normal and confirmed glaucoma cases (*set2*). 324 feature vectors corresponding to normal cases are used for training the classifier in both the experiments. The test set had 862 (300 normal + 234 suspect + 328 confirmed) images in (i) and 628 (300 normal + 328 confirmed) images in (ii).

The ROC plots for experiment (i) is presented in figure 9. It can be observed that the classification performance of RTD is significantly higher than HIC. The performance of HIC may improve further if the motion parameters are tuned for this descriptor. The sensitivity, specificity and AUC values for the two descriptors are shown in table 2. A high sensitivity of 0.97 is observed in detecting the glaucoma cases at a specificity of 0.87. It was found that, of all the detected abnormal cases, the suspect cases were correctly detected at a rate of 92 percent. Therefore, the proposed method is quite sensitive to detecting subtle variations due to the disease, which is desirable in a screening scenario.

In the second experiment, we assess the sensitivity of the system to confirmed cases of glaucoma. A high value of sensitivity for classification is expected as confirmed cases should be detected without fail in disease screening scenario. ROC plots for the experiment is shown in figure 10. Sensitivity of detection for RTD continues to be high while the specificity of detection has improved significantly when only confirmed glaucoma cases are considered. The respective metrics of classification can be observed in table 3. The best sensitivity of classification is found to be 1 against a specificity of 0.98. Performance of HIC is relatively lower as the GMP parameters are not tuned to this descriptor.

Global feature based techniques have also been proposed by Bock et al. [3]. They performed glaucoma detection on a dataset of 575 color retinal images. Only the confirmed cases of glaucoma were treated as abnormal. Several global image descriptors based on intensity, texture and spatial frequencies were used with SVM classifier for evaluation. Even though the datasets are different, for comparison, we report the results of a 5-fold cross validation analysis (similar to [3]) on *set2* consisting 952 images (624 normal + 328 confirmed glaucoma cases). It is evident from the performance figures in table 4 that our method shows significant improvement for normal and glaucoma image classification.

In another work, Bock et al. [2] tested the same set of

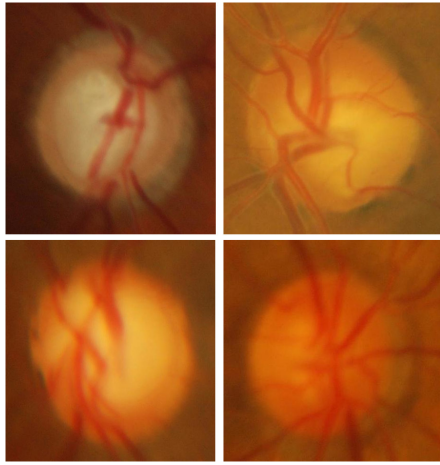


**Figure 11: Sample suspect glaucoma cases detected successfully by the proposed method.**

global image descriptors on a set of 200 retinal images. 100 images were used for training the classifier and the remaining for testing. The highest correct classification for a train-test cycle with multiple classifiers was observed as 83 percent. In comparison our highest classification accuracy is nearly 91 percent for a train-test cycle on a larger dataset (set 1 with 1186 images).

#### 4. CONCLUSION

Describing subtle variations in retinal structures using global image features for glaucoma detection is a challenging task. In this work, we propose a global feature for glaucoma detection at the image level. The proposed feature was used to design a glaucoma detection system. The system was shown to be able to distinguish between normal and glaucoma cases even when the decision on glaucoma was only at the 'suspect' level. Figure 11 depicts sample suspect cases that were detected with the proposed method. These are generally difficult cases to handle and hence the success of the system demonstrates the strength of the proposed global feature. The proposed feature was based on the GMP based image representation which was originally proposed for detecting the presence of localized high contrast lesions (hard exudates) against normal background in retinal images. The current work thus extends the scope of the GMP representation for detecting abnormalities caused by subtle morphological changes.

#### 5. ACKNOWLEDGMENT

The authors would like to thank Dr. R. Sharmila, Dr. P.S. Vivek and Dr. S. R. Krishnadas from Aravind Eye Hospitals, Madurai for providing annotations and knowledge about visual indicators of glaucoma in retinal images. This work was supported by the Department of Science and Technology, Government of India under Grant SR/ S3/ EECE / 0024 / 2009.

#### 6. REFERENCES

[1] M. D. Abramoff, W. L. M. Alward, E. C. Greenlee, L. Shuba, C. Y. Kim, J. H. Fingert, and Y. H. Kwon. Automated segmentation of the optic disc from stereo

color photographs using physiologically plausible features. *Investigative Ophthalmology and Visual Science*, 48:1665–1673, 2007.

- [2] R. Bock, J. Meier, G. Michelson, L. Nyúl, and J. Hornegger. Classifying glaucoma with image-based features from fundus photographs. *Proc. DAGM*, pages 355–364, 2007.
- [3] R. Bock, J. Meier, L. Nyúl, and G. Michelson. Glaucoma risk index: automated glaucoma detection from color fundus images. *Medical Image Analysis*, 14(3):471–481, 2010.
- [4] E. Corona, S. Mitra, M. Wilson, T. Krile, and Y. H. K. P. Soliz. Digital stereo image analyzer for generating automated 3-d measures of optic disc deformation in glaucoma. *IEEE Trans Med Imaging*, 21(10):1244–1253, 2002.
- [5] K. S. Deepak, N. K. Medathati, and J. Sivaswamy. Detection and discrimination of disease-related abnormalities based on learning normal cases. *Pattern Recogn.*, 45(10):3707–3716, Oct. 2012.
- [6] K. S. Deepak and J. Sivaswamy. Automatic assessment of macular edema from color retinal images. *Medical Imaging, IEEE Transactions on*, 31(3):766–776, march 2012.
- [7] G. D. Joshi, J. Sivaswamy, K. Karan, and S. R. Krishnadas. Optic disk and cup boundary detection using regional information. In *IEEE International Symposium on Biomedical Imaging (ISBI)*, pages 948–951, 2010.
- [8] G. D. Joshi, J. Sivaswamy, and S. R. Krishnadas. Optic disk and cup segmentation from monocular colour retinal images for glaucoma assessment. *IEEE Transactions on Medical Imaging*, 30(6):1192–1205, 2011.
- [9] J. Liu, D. Wong, J. Lim, H. Li, N. Tan, and T. Wong. Argali- an automatic cup-to-disc ratio measurement system for glaucoma detection and analysis framework. In *Proc. SPIE, Medical Imaging*, pages 72 603k–8, 2009.
- [10] J. Meier, R. Bock, G. Michelson, L. Nyúl, and J. Hornegger. Effects of preprocessing eye fundus images on appearance based glaucoma classification. *Proc. CAIP*, pages 165–172, 2007.
- [11] S. Philip, A. D. Fleming, K. A. Goatman, S. Fonseca, P. Mcnamee, G. S. Scotland, G. J. Prescott, P. F. Sharp, and J. A. Olson. The efficacy of automated disease/no disease grading for diabetic retinopathy in a systematic screening programme. *Br J Ophthalmol.*, 91(11):1512–1517, 2007.
- [12] C. Shyu, C. Brodley, A. Kak, A. Kosaka, A. Aisen, and L. Broderick. Local versus global features for content-based image retrieval. In *Content-Based Access of Image and Video Libraries, 1998. Proceedings. IEEE Workshop on*, pages 30–34, jun 1998.
- [13] Y. Wang, W. Tsu, and S. Lee. Illumination normalization of retinal images using sampling and interpolation. In *Proc. SPIE, Medical Imaging*, pages 500–507, 2001.